Adsorption (2011) 17: 583–593
DOI 10.1007/s10450-011-9331-9

Characterisation of hybrid xerogels synthesised in acid media using methyltriethoxysilane (MTEOS) and tetraethoxysilane (TEOS) as precursors

Xabier Rios · Paula Moriones · Jesús C. Echeverría · Asunción Luquín · Mariano Laguna · Julián J. Garrido

Received: 3 August 2010 / Accepted: 28 January 2011 / Published online: 12 February 2011

Abstract The mild synthetic conditions provided by the sol-gel process and the versatility of the colloidal state allow for the mixing of inorganic and organic components at the nanometre scale in virtually any ratio for the preparation of hybrid materials. Our interest in hybrid xerogels focuses on combining their porosity with other properties to prepare optic-fibre sensors. The specific aim of this paper is to synthesise hybrid xerogels in acid media using methyltriethoxysilane (MTEOS) and tetraethoxysilane (TEOS) as silica precursors and to investigate the effect of the MTEOS molar ratio on the structure and porous texture of xerogels. Gelation time exponentially increased as the MTEOS molar ratio increased. Increasing the MTEOS molar ratio yielded xerogels with lower density and lower particle size. The incorporation of MTEOS resulted in new FTIR bands at 1276 and 791 cm^{-1}, which was attributed to vibrational modes of methyl group. The band around 1092 cm^{-1} associated with siloxane bonds shifted to lower wavenumbers and split into two bands. The ^{29}Si spectra only showed the Q^n ($n = 2, 3, 4$) signal in xerogels with 0% MTEOS and the T^n ($n = 2, 3$) signal in xerogels with 100% MTEOS; hybrid xerogels showed both Q and T signals. From XRD peaks at 2θ around 9°, we inferred that xerogels (>70% MTEOS) consisted of nanocrystalline CH_3–$SiO_{3/2}$ species. Increasing the MTEOS molar ratio produced xerogels with lower pore volumes and lower average pore size. The integration of methyl groups on the surface decreased the surface polarity and, in turn, the characteristic energy.

Keywords Hybrid xerogels · Structure · Porous texture · TEOS · MTEOS

X. Rios · P. Moriones · J.C. Echeverría · J.J. Garrido (✉)
Departamento de Química Aplicada, Universidad Pública de Navarra, Campus Arrosadía, 31006 Pamplona, Spain
e-mail: j.garrido@unavarra.es

A. Luquín · M. Laguna
Instituto de Ciencia de Materiales de Aragón (CSIC), Departamento de Química Inorgánica, Universidad de Zaragoza, Zaragoza, Spain

1 Introduction

The sol-gel process has been widely used in the preparation of inorganic oxidic networks through the hydrolysis and polycondensation of alkoxides. Silica xerogels have applications in adsorption, separation media, sensors, drug-delivery supports, and oil-spill cleanup (Brinker and Scherer 1990). The sol-gel process offers some advantages over other procedures in obtaining ceramic materials, including (a) low-temperature synthesis, (b) high-purity materials, and (c) customisable porosity of xerogel products. The structure and porous texture of xerogels synthesised using tetraethoxysilane (TEOS) as a precursor depend on synthesis conditions, namely, pH, temperature, and the precursor:solvent:water molar ratio (Echeverria et al. 2010; Estella et al. 2007a, 2007b; Musgo et al. 2009). Porous texture is also affected by ageing and drying conditions (Estella et al. 2007a).

The versatility of the colloidal state allows for the mixing of inorganic and organic components at the nanometre scale in virtually any ratio for the preparation of hybrid materials (Sanchez and Ribot 1994; Sanchez et al. 2010). In sol-gel chemistry, $R_xSi(OR')_{4-x}$ alcoxysilanes are often employed, where R is any hydrolytically stable organic group covalently bonded to the polysiloxane network. Through hydrolysis and polycondensation of $Si(OR')_4$, SiO_2 xerogels are obtained. If $Si(OR')_4$ is replaced by $RSi(OR')_3$, a condensation site is blocked, and the average degree of cross-linking drops from four to three without taking into account

residual Si–OR′ and Si–OH groups in the final material. The hydrolysis rate generally depends on the type of precursors, and thus, reactive monomers are produced at different rates (Schmidt 1988). By mixing both precursors and changing the $RSi(OR')_3/Si(OR')_4$ molar ratio, control over the amount of organic groups in the inorganic matrix can be achieved. Alkyl or aryl R groups are interesting for several reasons. First, they allow easy modification of the silica network without introducing overly bulky or reactive organic groups. Second, they provide hydrophobicity to the resulting xerogel, and, third, they can serve as models for the study of sol-gel chemistry of more complex R substituents.

Our interest in hybrid xerogels hinges on combining their porosity with other properties (e.g., transparency, refractive index, ease of thin-film formation, and the ability to disperse other sensitive compounds in xerogel) to prepare optic-fibre sensors (Estella et al. 2010). The specific aim of this work is to synthesise hybrid xerogels in acid media using MTEOS and TEOS as silica precursors and to investigate the evolution of the structure, texture and surface chemistry of these materials. A xerogel synthesised at pH 4.5, 60 °C, and a 1:4.75:5.5 precursor:EtOH:water molar ratio was used as a reference.

2 Materials and methods

2.1 Xerogel synthesis

TEOS and MTEOS with purities of at least 98% were obtained from the Fluka Company (Switzerland). Absolute ethanol GR for analysis and hydrochloric acid GR were supplied by Merck (Darmstadt, Germany). Water was of MilliQ quality. The required amounts of precursors and ethanol were mixed using a magnetic stirrer in a 30-mL glass container. While stirring, the required amount of water was added drop-wise, and the pH of the solution was adjusted to 4.5 by adding 0.1-M HCl with an automated burette (Titrino 702 SM, Metrohm, Herisau, Switzerland). The sample containers were closed and stirred in an orbital shaker and then kept until gelation. The gels were covered with 5 mL of ethanol and allowed to age for seven days. Alcogels were dried at 22 ± 2 °C at atmospheric pressure.

2.2 Sample characterisation

Skeletal density was measured by helium pycnometry Accupyc 1330, Micromeritics (Norcross, USA). X-ray diffraction (XRD) spectra were acquired at ambient temperature using a Rigaku D-max instrument with a copper rotating anode and a graphite monochromator, which was used to select the $CuK_{\alpha 1/2}$ wavelength. The device was used at 40 kV and 80 mA. The measurements were carried out in step-scan mode for $5 \leq 2\theta \leq 60°$ in steps of 0.03° with a counting rate of 1 step s^{-1}. Micrographs were obtained by a field-emission scanning electron microscope (FE-SEM) from Carl Zeiss Ultra Plus (Germany). This apparatus allows the observation of samples without metallic layers. An InLens detector and a 2-kV working voltage were used. The xerogels morphology was studied by image analysis (NIS-Elements BR 3.2, NIKON, Tokyo, Japan).

Fourier-transformed infrared (FTIR) spectra were obtained using a Nicolet Avatar 360 FTIR spectrometer (Madison, USA). For each sample, 32 scans in the 4000–400 cm^{-1} spectral range were recorded with a resolution of 4 cm^{-1}. The KBr pressed-disc technique was used at two sample concentrations to record spectra in the regions of 4000–2200 and 2200–400 cm^{-1}, with 2 and 0.6 mg each dispersed in 200 mg of KBr. Discs were heated in a furnace at 150 °C overnight to minimise the water adsorbed on KBr and the samples (Madejova and Komadel 2001).

Simultaneous thermogravimetry and differential scanning calorimetry (TGA-DSC) analyses of xerogels were performed using a thermogravimetric analyser SETARAM, Mod. Setsys Evolution 1600 (Caluire, France), under an air atmosphere. Samples were placed in a platinum crucible, and the heating rate was 10 °C min^{-1}. A blank corresponding to a trial under the same conditions but without a sample was subtracted from each run.

The ^{29}Si CP MAS solid-state NMR was recorded on a Bruker AV-400 MHz spectrometer (Billerica, USA) operating at 79.5 MHz for ^{29}Si. Spectra were recorded at room temperature, with chemical shifts given in ppm relative to tetramethylsilane (TMS). The sample-rotation frequency was 5 kHz, and 800 scans were accumulated for each spectrum. The spectra were obtained using ^{1}H decoupling.

Nitrogen adsorption at −196 °C and CO_2 adsorption at 0 °C were measured using an ASAP 2010 volumetric adsorption analyser from Micromeritics (Norcross, USA). Approximately 100 mg of each sample was accurately weighed in an elongated Pyrex glass tube. Before adsorption analysis, the samples were outgassed for at least 15 h at 150 °C at the degassification port of the adsorption apparatus with a residual vacuum of 7×10^{-1} Pa. Specific surface areas were calculated from the N_2 adsorption data (molecular cross section 0.162 nm^2) by the BET method according to criteria described by Rouquerol et al. (1999) and by applying the DR method to CO_2 adsorption with a molecular cross-section of 0.170 nm^2. Micropore volumes were obtained by applying the DR method. Mesopore volumes were obtained from the difference between the amount of N_2 adsorbed at $p/p°$ 0.8 and 0.3. Total volume was determined from the amount adsorbed at $p/p°$ 1. Pore volumes were calculated using liquid-state densities for adsorbates of N_2 at 0.808 g cm^{-3} and CO_2 at 1.023 g cm^{-3} (CazorlaAmoros et al. 1996; Garrido et al. 1987).

3 Results and discussion

3.1 Gelation time

Figure 1 shows the variation in gelation time along with the molar ratio of MTEOS used during synthesis. Gelation time increased exponentially with the molar ratio of MTEOS ($R^2 = 0.991$). These results are consistent with those obtained for TEOS-MTEOS by Mendez-Vivar and Mendoza-Bandala (2000). In HCl-catalysed reactions, hydrolysis is faster than condensation (Devreux et al. 1990; Meixner and Dyer 1999), and alkyl-substituted trialkoxysilanes hydrolyse faster than the corresponding tetraalkoxysilanes (Himmel et al. 1990). In particular, MTEOS hydrolyses faster than the TEOS monomer during each sequential hydrolysis reaction (Fyfe and Aroca 1997; Jitianu et al. 2003). The replacement of the acidic conditions of an alkoxy by non-hydrolysable radicals leads to higher hydrolysis rates because the inductive effect of these radicals lowers the positive charge on the silicon and increases the negative charge on the oxygen atoms around the silicon atom as compared with TEOS (Devreux et al. 1990; Jitianu et al. 2003). Due to the fast hydrolysis rate, the formation of siloxane bonds controls the condensation rate, which in acidic media increases as a logarithm of time. The presence of methyl groups decreases the condensation rate because they reduce the net charge on the silicon atom, which is the key parameter for the nucleophilic condensation process above the isoelectric point (pH = 2) (Iler 1979). As MTEOS concentration increases, condensation kinetics slow down because the dimerisation rate of hydrolysed species from MTEOS is slower than that of species from TEOS (Fyfe and Aroca 1997).

3.2 Xerogel characterisation: helium density, XRD, FE-SEM, FTIR, TGA-DSC and NMR

3.2.1 Helium density

Helium density, also known as true or skeletal density, is obtained when the volume measured excludes the pores within the sample material (Webb and Orr 1997). The variation in the helium density of xerogels decreases linearly with the MTEOS molar ratio. The density of the xerogel prepared using TEOS as the only precursor was 1.83 g cm^{-3}, which was lower than that of cristobalite (2.334 g cm^{-3}) and vitreous silica (2.196 g cm^{-3}). The density of the xerogel synthesised from 100% MTEOS was 1.33 g cm^{-3}. The decrease in skeletal density can be attributed to the incorporation of methyl groups into the xerogel and to the reduction of cross-linking. MTEOS/TEOS copolymerisation tends to approximate a random copolymerisation, producing a matrix with a randomly distributed methyl functionality (Fyfe and Aroca 1997).

3.2.2 XRD analysis

Figure 2 shows the X-ray diffraction patterns for samples synthesised from 0%, 30%, 70%, and 100% MTEOS molar ratios. All patterns show one broad peak at 2θ around 23°, which is characteristic of amorphous silica (Garcia-Cerda et al. 2002; Kamiya et al. 1998). For MTEOS molar ratios of 70% and 100%, a distinct peak developed at $2\theta = 8.7°$ and 9.8°, respectively. Table 1 includes the values of the smaller ($2\theta_1$) and larger ($2\theta_2$) angles and their relative Bragg d-spacings (d_1 and d_2, respectively) and intensities (I_{r_1} and I_{r_2}, respectively).

The peak at the larger angle is associated with the spacing between silicon atoms connected by an oxygen bridge (Lana and Seddon 1998). This peak shifts from $2\theta = 23.2°$ for 0% MTEOS to $2\theta = 22.4°$ for 100% MTEOS. Correspondingly, the spacing between silicon atoms increased

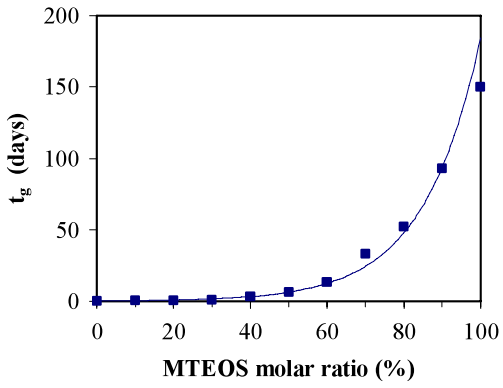

Fig. 1 Evolution of gelation time as a function of MTEOS molar ratio

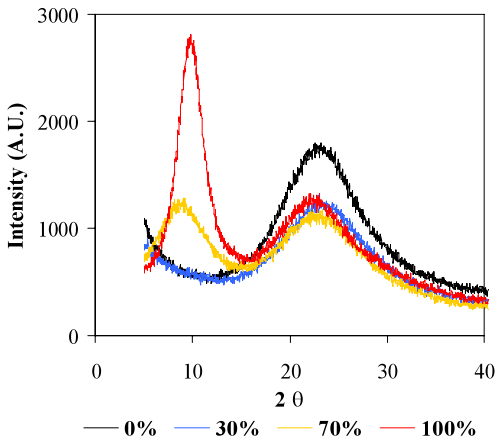

Fig. 2 X-ray diffraction patterns of the xerogels

Table 1 Bragg angles (2θ), band width at half height, d-spacing and relative intensity for $MTEOS_x/TEOS_{(100-x)}$ xerogels synthesised at pH 4.5

[MTEOS] (%)	2θ (°)	Δ_1 (°)	d_1 (nm)	I_{r_1}	$2\theta_2$ (°)	Δ_2 (°)	d_2 (nm)	I_{r_2}
0	–		–	–	23.1	8.7	0.39	1780
30	–		–	–	23.7	8.9	0.38	1200
70	8.7	5.2	0.10	1210	22.3	8.2	0.41	1260
100	9.8	2.8	0.91	2740	22.5	7.4	0.40	1110

from 0.39 nm for the silica xerogel synthesised from TEOS to 0.405 nm for 100% MTEOS. Apparently, the inductive effect of the methyl group decreases the net charge on the silicon atoms, which, in turn, results in larger bond distances.

The peak that appeared at the smaller angle shifted towards higher 2θ. The Bragg d-spacing decreased from 1.02 nm for 70% MTEOS to 0.92 nm for 100% MTEOS. The intensity of d_1 relative to the intensity of d_2 doubled when the organic character of the matrix was increased from 70% to 100% MTEOS. The origin of this peak is still controversial. It has been assigned to the presence of four-fold siloxane rings (Fidalgo and Ilharco 2001; Kamiya et al. 1998; Yoshino et al. 1990), but it may originate from a discrete structural unit in the matrix based on an octameric silicon arrangement consisting of nanocrystalline CH_3–$SiO_{3/2}$ species (Lana and Seddon 1998; Orel et al. 2005).

3.2.3 FE-SEM

Figure 3 shows FE-SEM micrographs of xerogels synthesised with 0%, 30%, and 70% MTEOS. Xerogel synthesised with TEOS presented a very rough surface (Fig. 3(a)). Xerogel obtained with 30% of MTEOS (Fig. 3(b)) showed a smoother surface. This effect was more pronounced in xerogels prepared with more than 70% of MTEOS (Fig. 3(c)). The entry of methyl groups into the network leads to xerogels with minor cross-linking since the methyl groups are not hydrolysable, less dense but more compacts. The reduction of the cross-linked leads to less rigid structures, where packing of the siloxanic chains must be higher. That's why xerogels with more content in MTEOS should have fewer empty voids and a more reduced porosity.

3.2.4 FTIR

Figure 4 includes the infrared spectra of samples synthesised from MTEOS/TEOS mixtures containing 0%, 30%, 60%, 70%, and 100% MTEOS in two wavenumber ranges, namely, 4000–2750 cm^{-1} and 1600–400 cm^{-1}. The 2750–1600 cm^{-1} range was not included due to its lack of relevant bands. For xerogel synthesised from TEOS (0% MTEOS), the three characteristic IR bands attributed to the different vibrational modes of the silica network can be observed at 1092, 802, and 459 cm^{-1} (Fidalgo and Ilharco 2004; Innocenzi et al. 2003). The most intense band at 1092 cm^{-1} is attributed to the asymmetric stretching vibration of the Si–O–Si bond, which forms the skeletal SiO_2 network (Fi-

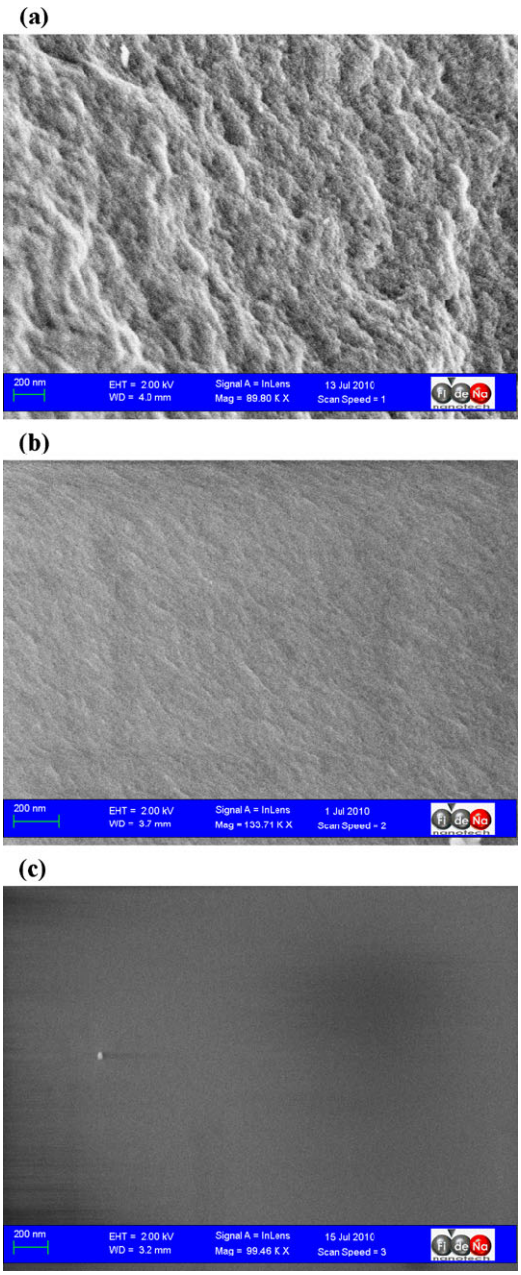

Fig. 3 FE-SEM micrographs of hybrid xerogels with different percentages of MTEOS: (**a**) 0%; (**b**) 30%; and (**c**) 70%

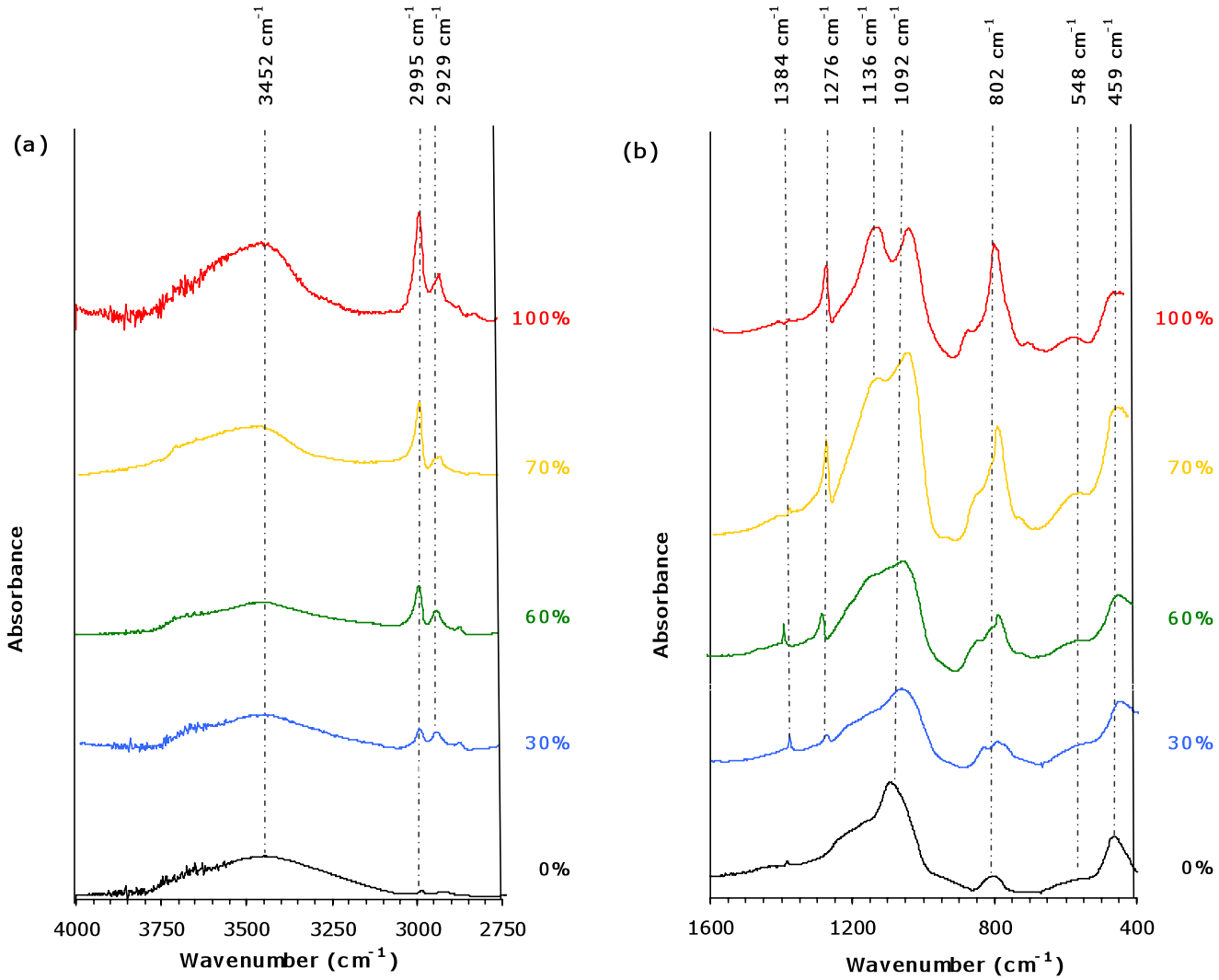

Fig. 4 Infrared spectra in two wavenumber ranges: (**a**) 4000–2750 cm^{-1} and (**b**) 1600–400 cm^{-1}

dalgo and Ilharco 2004; Innocenzi 2003). The bands at 802 and 459 cm^{-1} are assigned to the bond-bending and bond-rocking vibrations, respectively, of the Si–O bonds in the three-dimensional SiO_2 network. The shoulder at 550 cm^{-1} is assigned to the presence of 4-fold siloxane rings in the xerogel (Kamiya et al. 1998; Yoshino et al. 1990). In addition to the characteristic bands of SiO_2 materials, a broad band between 3750 and 3000 cm^{-1} is attributed to the different contributions of isolated, geminal, vicinal and H-bonding silanol groups (Innocenzi et al. 2003). The shoulder at 950 cm^{-1} is due to the Si–OH and Si–O– groups on the xerogel surface. Two bands of low intensity at 2995 and 2929 cm^{-1} were assigned to non-hydrolysed ethoxy groups.

The FTIR spectra of hybrid organic-inorganic xerogels show remarkable differences when compared to the spectrum of xerogel synthesised from TEOS. The incorporation of a methyl group into the xerogel structure results in the appearance of distinct peaks corresponding to the different vibrational modes of Si–CH_3 bonds, including (a) out-of-phase or asymmetric CH_3 stretching vibration at 2976 ± 2 cm^{-1}, (Murashkevich et al. 2008) in-phase or symmetric CH_3 stretching vibration at 2922 ± 5 cm^{-1}, (b) in-phase deformation at 1385 ± 0 cm^{-1}, and (c) in-phase rocking vibration at 780 ± 8 cm^{-1}. The band at 1277 ± 2 cm^{-1} is attributed to the symmetric deformation of Si–CH_3 bond. As the molar ratio of MTEOS increases, the Si–O–Si asymmetric stretching and rocking vibration bands at 1092 and 459 cm^{-1} shift to lower wavenumbers, indicating that bond energy decreases with increasing MTEOS content. This red-shift supports the XRD observation that the Si–O–Si bond distance increases with the MTEOS molar ratio. In addition to shifting to lower wavenumbers, a distinct peak appeared at 1136 cm^{-1} for 70 and 100% MTEOS. Although vibrational modes in the 1200–1000 cm^{-1} range have been extensively reported, the assignment of vibrational modes in this region is still controversial. However, this peak cor-

relates with the XRD peak that developed at 2θ between 8.7° and 9.8°; moreover, its intensity also increased with MTEOS molar ratio content. Therefore, this peak seems to be related to an octameric silicon arrangement.

Increasing the MTEOS molar ratio resulted in major spectral changes in the ranges of 1250–900 cm^{-1} and 900–700 cm^{-1}. The 1092 cm^{-1} band, which is associated with a transverse-optical (TO)-coupling Coulomb interaction (Almeida and Pantano 1990), shifted to 1024 cm^{-1} for MTEOS molar ratios higher than 80%. The shoulder associated with the band at 1136 cm^{-1}, which is related to the longitudinal-optical (LO) component, became a distinct band and shifted to lower wavenumbers, specifically 1136 cm^{-1} for MTEOS molar ratios higher than 70%. The shift of the TO and LO components to lower wavenumbers is related to smaller siloxane rings with larger Si–O bonds (Almeida and Pantano 1990; Ilharco et al. 2007).

3.2.5 TGA and DSC analyses

TGA and DSC analyses were performed to check the stability of the xerogels and to evaluate the effect of the incorporation of MTEOS in the structure. Figure 5 shows the (a) TGA and (b) DSC curves of xerogels synthesised from MTEOS molar ratios ranging from 0 to 100%. The TGA curves show three major steps as well as the contribution of each step to the total weight loss with varying MTEOS content at (a) $T < 200\,°C$, (b) $200 < T < 400\,°C$, and (c) $400 < T < 800\,°C$. The first range, which includes temperatures up to 200 °C, is endothermic (Fig. 5(b)) and mainly corresponds to the removal of water and ethanol trapped in the pores. The percentage varies between 17.5% for the sample synthesised with 100% TEOS and 7.0% for that obtained with 50% MTEOS. The remainder of the sample mass loss variations were below 2%. The surface silanol groups act as adsorption centres with greater affinity for water and polar solvents; the slope of the curves and the magnitude of the changes in mass suggest that the surface polarity of hybrid materials decreases with the MTEOS molar ratio.

The second temperature range is between 180 °C and 400 °C. The mass variations are small, and the process is endothermic. For MTEOS molar ratios smaller than 50%, the mass losses are 3% and lower for higher percentages. This loss of mass may be due to the loss of water caused by the condensation of the surface silanol groups.

The interval from 400 °C to 800 °C is the third range. For percentages of MTEOS equal to less than 30%, only a signal is observed, which begins between 343 °C for the xerogel with 10% MTEOS and 514 °C for 20% MTEOS. The maximum variations in mass for these compositions occur at 422 and 541 °C, respectively. The percentage of lost relative mass is less than 4% for MTEOS molar ratios between 40% and 90%. In addition, two signals appear; the first begins at 413 °C for the sample with 90% MTEOS and at 536 °C for the sample with 50% MTEOS. The second peak begins at 650 °C. Curiously, the starting temperature of the second peak barely changes with MTEOS percentage, with the maximum variation in mass at 710 °C. Figure 5(b) shows that the changes are exothermic and on the order of kJ g^{-1}. This energy corresponds to breaking bonds. Because the analyses were performed in air, one would expect that the loss of mass corresponds to the oxidation of methyl groups to CO_2 and water. Because these peaks overlap, the mass loss corresponds to the interval between 400 °C and 800 °C. These losses range from 4.7% for the sample with 40% MTEOS to 13.8% for that with 90% MTEOS. Although the peaks between 400 °C and 800 °C are due to the oxidation of the methyl group, the differences between them can be attributed to the existence of two types of methyl groups, namely, the more superficial groups and those occluded in the xerogel matrix.

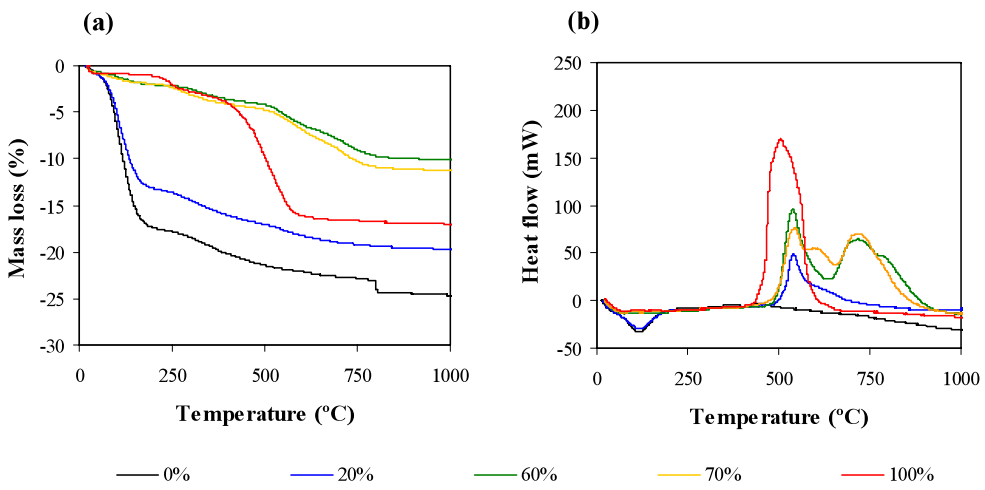

Fig. 5 (**a**) TGA and (**b**) DSC silica xerogels for different MTEOS molar ratios

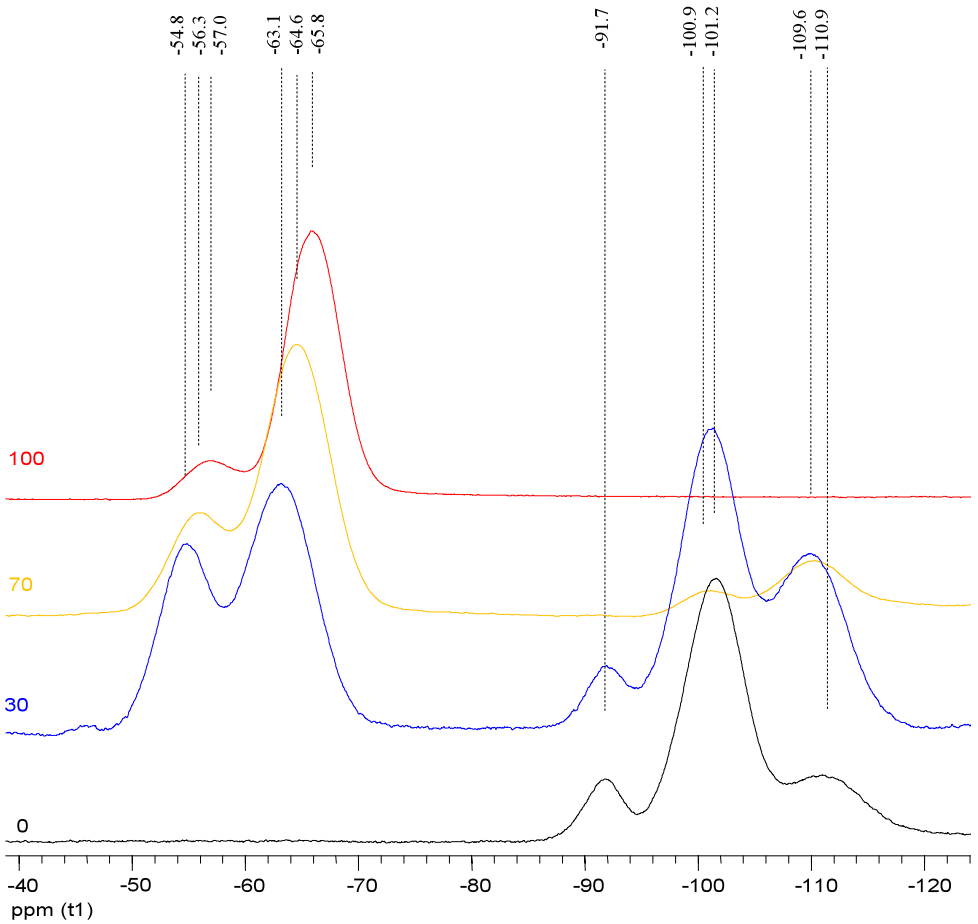

Fig. 6 ^{29}Si NMR of the xerogels

Table 2 Signals for the ^{29}Si NMR spectra for MTEOS$_x$/TEOS$_{(100-x)}$ xerogels synthesised at pH 4.5

MTEOS (%)	^{29}Si NMR (ppm)	
0	-91.7 (Q^2)	
	-101.1 (Q^3)	
	-110.9 (Q^4)	
30	-91.7 (Q^2)	-54.8 ($T^2 + T^3$)
	-101.3 (Q^3)	-63.1 (T^3)
	-109.9 (Q^4)	
70	-100.9 (Q^3)	-56.3 ($T^2 + T^3$)
	-109.6 (Q^4)	-64.6 (T^3)
100		-57.0 ($T^2 + T^3$)
		-65.8 (T^3)

3.2.6 NMR

The ^{29}Si NMR spectra obtained in this work for the TEOS and MTEOS xerogels (0% and 100%, respectively) are in accordance with previously described xerogels developed in acid media (Kamiya et al. 1998; Orel et al. 2005) (Fig. 6 and Table 2). In the NMR spectra of the xerogels obtained with different amounts of TEOS and MTEOS (i.e., 30% and 70% molar ratio MTEOS), a displacement of the signals is observed. This shift is present in both groups at -100 ppm for the TEOS signals and at -60 ppm for the MTEOS signals. In both cases, when the amount of TEOS decreases, the signals are high-field displaced. According to the data obtained by Orel et al., the MTEOS signals at -54.8 ppm (30%), -56.3 ppm (70%), and -57.0 ppm (100%) are related to the $T^2 + T^3$ units, while the signals at -63.1 ppm (30%), -64.6 ppm (70%), and -65.8 ppm (100%) are due to the T^3 units. Therefore, as the amount of MTEOS increases, the signal due to the T^3 units increases, and a peak at 2θ 9.7° develops. It is possible to explain the behaviour of the TEOS signals by considering the study by Kamiya et al. (1998). The xerogels presented in our study are prepared in acid media, which is the reason that the main signal in the TEOS zone of the spectrum is at -101 ppm. Note that this corresponds to the Q^3 species, which is the main species in this media. The other two species found in these gels are the Q^2 species, which appears at -91.7 ppm (0%) and -91.7 ppm (30%), and the Q^4 species, which appears at -110.9 ppm (0%) and -109.9 ppm (30%). In ^{29}Si NMR studies, the classical notations are T for silicon with three oxygen-bridging

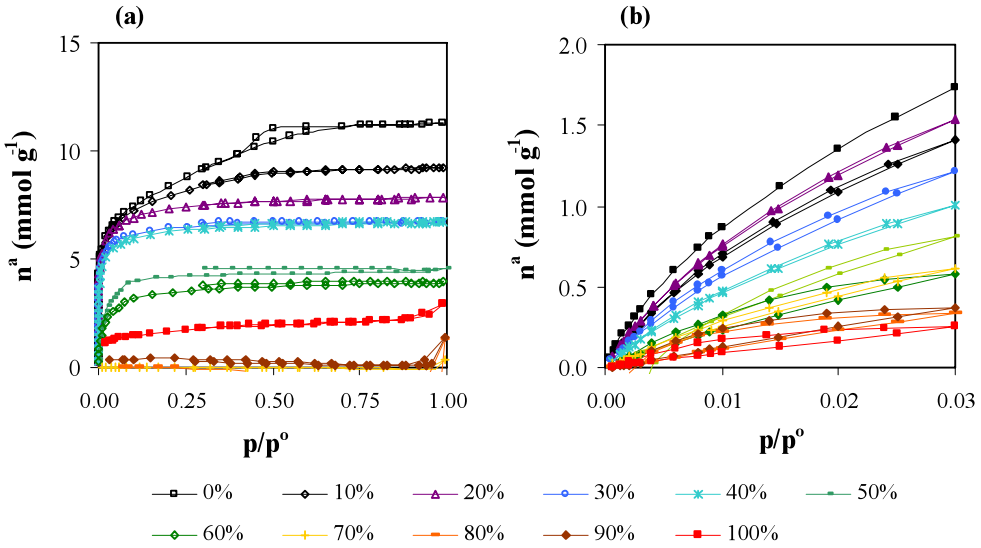

Fig. 7 Adsorption isotherms: (**a**) N_2 at −196 °C and (**b**) CO_2 at 0 °C

Table 3 Textural parameters for MTEOS/TEOS xerogels synthesised at pH 4.5

MTEOS (%)	$a_{BET\ (N_2)}$	$a_{DR(CO_2)}$	$V_{mi\ (N_2)}$	$V_{mi\ (CO_2)}$	$V_{meso\ (N_2)}$ [a]	$V_{T\ (N_2)}$
	($m^2\ g^{-1}$)		($cm^3\ g^{-1}$)			
0	673	395	0.240	0.158	0.070	0.391
10	624	334	0.247	0.134	0.025	0.319
20	616	361	0.238	0.145	0.009	0.271
30	550	293	0.230	0.117	0.005	0.234
40	517	248	0.230	0.100	0.008	0.232
50	324	238	0.153	0.096	0.005	0.157
60	266	158	0.110	0.063	0.009	0.136
70	[b]	164	[b]	0.066	[b]	[b]
80	[b]	132	[b]	0.053	[b]	[b]
90	[b]	168	[b]	0.067	[b]	[b]
100	[b]	82	[b]	0.033	[b]	[b]

[a]Deduced by difference between the amount of N_2 adsorbed in the relative pressure range 0.3–0.8

[b]These simples did not adsorb N_2

atoms and Q for silicon with four oxygen-bridging atoms (Brunet 1998; Van Nieuwenhuyse et al. 2008).

3.3 Porous texture

The increase in the MTEOS percentage used in the synthesis leads to xerogels with different porosities and lower skeletal density due to the incorporation of methyl groups and the reduction of cross-linking. Figure 7 shows the N_2 (−196 °C) and CO_2 (0 °C) adsorption isotherms of the xerogels obtained with different MTEOS molar ratios. According to IUPAC classification, the N_2 adsorption isotherm at −196 °C of the xerogel prepared with 0% MTEOS is type I–IV (Fig. 7(a)). The adsorption branch of this xerogel corresponds to type I, and the small hysteresis loop is characteristic of type-IV isotherms. When the molar ratio of MTEOS increases, the amount of adsorbed N_2 decreases, the knees of isotherms become sharper, the hysteresis loop disappears, and the isotherms plateau between $p/p°$ 0.4 and 1.0 (type-I isotherm). For MTEOS molar ratios above 70%, the xerogels did not absorb N_2. When the proportion of MTEOS was increased, the amount of CO_2 adsorbed decreased (Fig. 7(b)). Hysteresis loops were observed for molar percentages above 40%. The fact that all xerogels adsorbed CO_2 (0 °C), whereas samples synthesised with MTEOS molar ratios above 70% did not adsorb N_2 (−196 °C), which indicates the presence of micropores smaller than 0.7 nm.

Table 3 includes textural parameters obtained from N_2 and CO_2 adsorption. Increasing MTEOS content in the synthesis mixture results in xerogels with smaller specific surface areas. When nitrogen was used as the adsorbate, the decrease was more marked for MTEOS molar ratios higher than 40%. For MTEOS percentages above 70%, a_{BET} could not be measured because the xerogels did not adsorb N_2. Specific surface areas obtained by the DR method from CO_2 adsorption were smaller than a_{BET} deduced from N_2 adsorp-

tion, but the difference decreased with the initial percentage of MTEOS.

As was described for specific surface areas, pore volumes decreased with increasing MTEOS molar ratios. For percentages up to 20% MTEOS, the total pore volume, $V_{T(N_2)}$, is greater than $V_{mi(N_2)}$, which is greater than $V_{mi(CO_2)}$. This finding confirms the presence of meso- and micropores (both narrow and wide). Between molar ratios of 30% and 60%, $V_{T(N_2)}$ is similar to $V_{mi(N_2)}$, implying a loss of mesoporosity. In addition, $V_{mi(N_2)}$ is higher than $V_{mi(CO_2)}$; consequently, these xerogels maintain two types of microporosity.

The characteristic curves provided supplementary information on the adsorption process (Cazorla-Amoros et al. 1998; Garrido et al. 1987; Lozano-Castelló et al. 2004) and can be expressed as follows.

$$\frac{V}{V^\circ} = e^{-(\frac{A}{E\beta})^2} \tag{1}$$

where V is the volume adsorbed at a given relative pressure, V° is the micropore volume, A is the affinity or differential free energy of adsorption ($A = RT\ln(p^\circ/p)$), E is the characteristic free energy of adsorption for a given system, and β is the similarity factor, which is 0.33 and 0.46 for N_2 and CO_2, respectively. Figure 8 includes three examples of characteristic curves obtained for samples containing 0%, 30%, and 60% MTEOS. These xerogels cover the different porosity types found in xerogels. In the case of xerogels synthesised with 0% to 30% MTEOS, the characteristic curves of N_2 and CO_2 connect, although kinetic constraints exist for N_2 adsorption at $(A/\beta)^2 > 400$ kJ^2 mol^{-2}. The characteristic curves have a unique slope and deviate upwards. The porosity of these samples was well-developed and contains some amount of microporosity (both wide and narrow) and mesoporosity. For xerogels synthesised with 30% to 60% MTEOS, the characteristic curves of N_2 and CO_2 do not connect due to kinetic restrictions under N_2 adsorption. Xerogels obtained from MTEOS molar ratios in the range of 70–100% have a quite narrow microporosity, and N_2 adsorption exhibits activated diffusion (see Table 3).

Detailed analyses of the slope of characteristic curves corresponding to CO_2 adsorption provide further information (Fig. 8). The slopes range between -1.6×10^{-3} mol^2 kJ^{-2} (0% MTEOS) and -2.4×10^{-3} mol^2 kJ^{-2} (100% MTEOS). Therefore, an increasing of MTEOS produces bigger slopes. The slope of the characteristic curve is inversely related to the square of the characteristic energy (see (1)), which is in turn related to the adsorbent-adsorbate interaction and thus to the pore average size in cases where physisorption dominates the adsorption process. In other words, an increase in the absolute magnitude of the slope should indicate that the addition of MTEOS to the mixture of precursors leads to xerogels with larger average pore size. However, the adsorption isotherms contradict this hypothesis. Increasing the MTEOS molar ratio produced xerogels with smaller pore volume and lower average pore size (Fig. 7 and Table 3). On the other hand, the FTIR spectra demonstrate the incorporation of methyl groups into xerogel and the modification of siloxane bonds. In addition, the methyl groups on the surface decrease the surface polarity, which results in lower characteristic energy. In short, MTEOS gives rise to xerogels that are less polar than those obtained from TEOS and, consequently, have less adsorbent-adsorbate chemical interaction and lower characteristic energy.

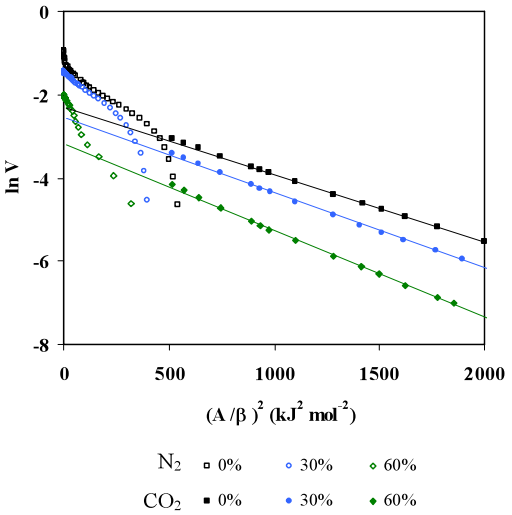

Fig. 8 Characteristic curves for adsorption of N_2 at −196 °C and CO_2 at 0 °C

4 Conclusions

Increasing the MTEOS molar ratio exponentially increased gelation time and yielded xerogels with lower helium density and particle size. Xerogels were amorphous, though a distinct XRD-peak developed at around $2\theta \sim 9°$, which is assigned to the presence of four-fold siloxane rings but may originate from a discrete structural unit in the matrix based on an octameric silicon arrangement (>70% MTEOS) consisting of nanocrystalline CH_3–$SiO_{3/2}$ species. The incorporation of MTEOS results in new FTIR bands at 1276 cm^{-1} and 791 cm^{-1}, which are attributed to the vibrational modes of Si–CH_3. Moreover, the band around 1092 cm^{-1} associated with siloxane bonds shifted to lower wavenumbers and split into two bands. ^{29}Si spectra only show the Q^n ($n = 2, 3, 4$) signal in xerogels with 0% MTEOS and the T^n ($n = 2, 3$) signal in xerogels with 100% MTEOS; meanwhile, hybrid xerogels show both Q and T signals. Increasing the MTEOS molar ratio produced xerogels with smaller pore volume and lower average pore size. The integration of

methyl groups on the surface decreases the surface polarity and, in turn, the characteristic energy.

Acknowledgements This work was supported by the Ministerio de Ciencia e Innovación (CTQ2009-07993). Xabier Rios and Paula Moriones are thankful to the "Departamento de Industria y Tecnología, Comercio y Trabajo" of Navarre Government for a fellowship.

References

Almeida, R.M., Pantano, C.G.: Structural investigation of silica-gel films by infrared-spectroscopy. J. Appl. Phys. **68**, 4225–4232 (1990)

Brinker, C.J., Scherer, G.W.: Sol-Gel Science: The Physics and Chemistry of Sol-Gel Processing. Academic Press, New York (1990)

Brunet, F.: Polymerization reactions in methyltriethoxysilane studied through ^{29}Si NMR with polarization transfer. J. Non-Cryst. Solids **231**, 58–77 (1998)

Cazorla-Amoros, D., Alcaniz-Monge, J., de la Casa-Lillo, M.A., Linares-Solano, A.: CO_2 as an adsorptive to characterize carbon molecular sieves and activated carbons. Langmuir **14**, 4589–4596 (1998)

CazorlaAmoros, D., AlcanizMonge, J., LinaresSolano, A.: Characterization of activated carbon fibers by CO_2 adsorption. Langmuir **12**, 2820–2824 (1996)

Devreux, F., Boilot, J.P., Chaput, F., Lecomte, A.: Sol-gel condensation of rapidly hydrolyzed silicon alkoxides—a joint Si-29 NMR and small-angle X-ray-scattering study. Phys. Rev. A **41**, 6901–6909 (1990)

Echeverria, J.C., Estella, J., Barberia, V., Musgo, J., Garrido, J.J.: Synthesis and characterization of ultramicroporous silica xerogels. J. Non-Cryst. Solids **356**, 378–382 (2010)

Estella, J., de Vicente, P., Echeverria, J.C., Garrido, J.J.: A fibre-optic humidity sensor based on a porous silica xerogel film as the sensing element. Sens. Actuators B, Chem. **149**, 122–128 (2010)

Estella, J., Echeverria, J.C., Laguna, M., Garrido, J.J.: Effects of aging and drying conditions on the structural and textural properties of silica gels. Microporous Mesoporous Mater. **102**, 274–282 (2007a)

Estella, J., Echeverria, J.C., Laguna, M., Garrido, J.J.: Silica xerogels of tailored porosity as support matrix for optical chemical sensors. Simultaneous effect of pH, ethanol : TEOS and water : TEOS molar ratios, and synthesis temperature on gelation time, and textural and structural properties. J. Non-Cryst. Solids **353**, 286–294 (2007b)

Fidalgo, A., Ilharco, L.M.: The defect structure of sol-gel-derived silica/polytetrahydrofuran hybrid films by FTIR. J. Non-Cryst. Solids **283**, 144–154 (2001)

Fidalgo, A., Ilharco, L.M.: Correlation between physical properties and structure of silica xerogels. J. Non-Cryst. Solids **347**, 128–137 (2004)

Fyfe, C.A., Aroca, P.P.: A kinetic analysis of the initial stages of the sol-gel reactions of methyltriethoxysilane (MTES) and a mixed MTES/tetraethoxysilane system by high-resolution Si-29 NMR spectroscopy. J. Phys. Chem. B **101**, 9504–9509 (1997)

Garcia-Cerda, L.A., Mendoza-Gonzalez, O., Perez-Robles, J.F., Gonzalez-Hernandez, J.: Structural characterization and properties of colloidal silica coatings on copper substrates. Mater. Lett. **56**, 450–453 (2002)

Garrido, J., Linares-Solano, A., Martin-Martinez, J.M., Molina-Sabio, M., Rodriguez-Reinoso, F., Torregrosa, R.: Use of N_2 vs CO_2 in the characterization of activated carbons. Langmuir **3**, 76–81 (1987)

Himmel, B., Gerber, T., Burger, H.: Waxs-investigations and saxs-investigations of structure formation in alcoholic SiO_2 solutions. J. Non-Cryst. Solids **119**, 1–13 (1990)

Iler, R.K.: The Chemistry of Silica. Wiley, New York (1979)

Ilharco, L.M., Fidalgo, A., Farinha, J.P.S., Martinho, J.M.G., Rosa, M.E.: Nanostructured silica/polymer subcritical aerogels. J. Mater. Chem. **17**, 2195–2198 (2007)

Innocenzi, P.: Infrared spectroscopy of sol-gel derived silica-based films: a spectra-microstructure overview. J. Non-Cryst. Solids **316**, 309–319 (2003)

Innocenzi, P., Falcaro, P., Grosso, D., Babonneau, F.: Order-disorder transitions and evolution of silica structure in self-assembled mesostructured silica films studied through FTIR spectroscopy. J. Phys. Chem. B **107**, 4711–4717 (2003)

Jitianu, A., Britchi, A., Deleanu, C., Badescu, V., Zaharescu, M.: Comparative study of the sol-gel processes starting with different substituted Si-alkoxides. J. Non-Cryst. Solids **319**, 263–279 (2003)

Kamiya, K., Dohkai, T., Wada, M., Hashimoto, T., Matsuoka, J., Nasu, H.: X-ray diffraction of silica gels made by sol-gel method under different conditions. J. Non-Cryst. Solids **240**, 202–211 (1998)

Lana, S.L.B., Seddon, A.B.: X-ray diffraction studies of sol-gel derived ORMOSILs based on combinations of tetramethoxysilane and trimethoxysilane. J. Sol-Gel Sci. Technol. **13**, 461–466 (1998)

Lozano-Castelló, D., Cazorla-Amorós, D., Linares-Solano, A.: Usefulness of CO2 adsorption at 273 K for the characterization of porous carbons. Carbon **42**, 1233–1242 (2004)

Madejova, J., Komadel, P.: Baseline studies of the clay minerals society source clays: infrared methods. Clays Clay Miner. **49**, 410–432 (2001)

Meixner, D.L., Dyer, P.N.: Influence of sol-gel synthesis parameters on the microstructure of particulate silica xerogels. J. Sol-Gel Sci. Technol. **14**, 223–232 (1999)

Mendez-Vivar, J., Mendoza-Bandala, A.: Spectroscopic study on the early stages of the polymerization of hybrid TEOS-RSi (OR′)(3) sols. J. Non-Cryst. Solids **261**, 127–136 (2000)

Murashkevich, A., Lavitskaya, A., Barannikova, T., Zharskii, I.: Infrared absorption spectra and structure of TiO_2-SiO_2 composites. J. Appl. Spectrosc. **75**, 730–734 (2008)

Musgo, J., Echeverria, J.C., Estella, J., Laguna, M., Garrido, J.J.: Ammonia-catalyzed silica xerogels: Simultaneous effects of pH, synthesis temperature, and ethanol:TEOS and water:TEOS molar ratios on textural and structural properties. Microporous Mesoporous Mater. **118**, 280–287 (2009)

Orel, B., Jese, R., Vilcnik, A., Stangar, U.L.: Hydrolysis and solvolysis of methyltriethoxysilane catalyzed with HCl or trifluoroacetic acid: IR spectroscopic and surface energy studies. J. Sol-Gel Sci. Technol. **34**, 251–265 (2005)

Rouquerol, F., Rouquerol, J., Sing, K.: Adsorption by Powders and Porous Solids. Academic Press, San Diego (1999)

Sanchez, C., Ribot, F.: Design of hybrid organic-inorganic materials synthesised via sol-gel chemistry. New J. Chem. **18**, 1007–1047 (1994)

Sanchez, C., Rozes, L., Ribot, F., Laberty-Robert, C., Grosso, D., Sassoye, C., Boissiere, C., Nicole, L.: "Chimie douce": A land of opportunities for the designed construction of functional inorganic and hybrid organic-inorganic nanomaterials. C. R., Chim. **13**, 3–39 (2010)

Schmidt, H.: Chemistry of material preparation by the sol-gel process. J. Non-Cryst. Solids **100**, 51 (1988)

Van Nieuwenhuyse, P., Bounor-Legare, V., Boisson, F., Cassagnau, P., Michel, A.: Hydrolysis-condensation reactions of diethylphosphato-ethyltriethoxysilane with tetraethoxysilane studied by ^{29}Si-NMR: Solvent and phosphonate catalytic effect. J. Non-Cryst. Solids **354**, 1654–1663 (2008)

Webb, P.A., Orr, C.: Analytical Methods in Fine Particle Technology. Micromeritics Instrument Corporation, Norcross (1997)

Yoshino, H., Kamiya, K., Nasu, H.: IR study on the structural evolution of sol-gel derived SiO_2 gels in the early stage of conversion to glasses. J. Non-Cryst. Solids **126**, 68–78 (1990)